BeBeC-2024-S03

EXPERIMENTAL VALIDATION OF CLEAN-SC FOR THE DETERMINATION OF DIRECTIVITY OF ENGINE NOISE SOURCES

Jared Vermeulen[1], Roberto Merino-Martínez[1], Pieter Sijtsma[1,2] and Mirjam Snellen[1]
[1]Faculty of Aerospace Engineering, Delft University of Technology
Kluyverweg 1, 2629 HS Delft, The Netherlands.

[2]PSA3, De Punt, 9493 TE, The Netherlands

Abstract

Turbofan engines are still one of the loudest noise sources of modern commercial aircraft. Noise radiation from the engine is highly directional and it is, therefore, important to obtain this directivity pattern from microphone-array data from static engine noise tests. Recently, Sijtsma has recently shown that the deconvolution method CLEAN-SC is able to break down engine noise sources and that it is capable of determining the directivity of these sources in the far field using measurements of a DGEN380 static engine test. This study further investigates this capability of CLEAN-SC by performing acoustic experiments under controlled conditions in the anechoic chamber at the faculty of applied sciences at Delft University of Technology. The experiments consist of a variety of tests with 2 different speakers placed inside an aluminum cylindrical pipe simulating an engine. In these experiments, the location and directivity of the individual noise sources can be measured separately, so that the CLEAN-SC results can be compared to the ground-truth reference. Moreover, the results are also compared with other acoustic imaging methods, such as DAMAS and conventional beamforming.

Nomenclature

A	Source power
c	Speed of sound
$\mathbf{C}$	Cross-spectral matrix
d	Microphone spacing
$\mathbf{D}$	Degraded CSM
e	Snapshot number
f	Frequency
$g_{j,n}$	Steering vector
h_j	Source component
i	Imaginary unit
J	Number of grid points
K	Number of sources
l	Number of iterations
N_{mic}	Number of microphones
$N_{mic,sec}$	Number of microphones in a section
$\mathbf{p}$	Pressure amplitudes per microphone
$\mathbf{w}_j$	Weighted steering vector
$\mathbf{x}$	Equivalent source distribution
$\mathbf{x}_n$	Vector of microphone positions
X	X-location in grid
$\mathbf{y}$	Source power output
Δt	Time delay
Δ_N	Difference between two breakdowns
λ	Wavelength
ϕ	Loop gain
ξ_j	Scan point

1 INTRODUCTION

Due to the increasing number of people living close to airports [9] combined with the increasing number of annual flights, more people suffer from noise pollution caused by aircraft than ever before, which makes it a relevant topic to investigate. One of the loudest sources of aircraft noise originates from the engines [3]. Noise radiation from an aircraft engine is highly directional and it is, therefore, important to obtain this directivity pattern from static engine noise tests, using microphone-array data.

Currently, in static engine noise testing, the most common ways to process microphone array data are conventional frequency domain beamforming (CFDBF) [12] and integration methods [7], but there are several other advanced methods to process acoustic microphone data with varying degree of accuracy and required computational time [6]. These methods are applied to the microphone array data to obtain an average-level breakdown. This means that the average level of the microphone array is written as a summation of the different sources present. However, using these methods the directivity of the individual sources typically remains unknown [13]. There are advanced methods that can perform the breakdown including directivity, such as SODIX [8] and AFINDS [14]. These techniques rely on inverse methods, which makes their implementation not straightforward. An alternative method has been recently proposed by Sijtsma, which employs CLEAN-SC [11] to process microphone-array data of static engine noise tests to also account for directivity. It was demonstrated that CLEAN-SC is capable of such a noise breakdown using test data of a DGEN380 turbofan engine [13]. The directivity results are plausible, but, since the ground-truth levels for such turbofan engine are unknown, further validation that CLEAN-SC is capable of performing a directivity breakdown with a reference noise source of known characteristics is required. Hence, a well-controlled experiment to validate this capability of CLEAN-SC is presented here.

The experimental setup to obtain the data is discussed in section 2. Afterwards, the methods to analyse this data are explained in section 3. Subsequently, the results of the analysis are presented and discussed in section 4. Finally, the conclusions are given in section 5.

2 EXPERIMENTAL SETUP

The objective of the experiment is to perform reference measurements, for which the location and directivity of the sources can be measured separately so that the ground-truth results can be compared to the outcome of the deconvolution tool CLEAN-SC. The experiments are performed in the anechoic chamber at the faculty of applied sciences at the Delft University of Technology, to minimize background noise levels and sound reflections. The experiment consists of a cylindrical aluminum pipe with two Visaton K 50 SQ speakers [15] inside as reference known sound signals, to simulate a static engine test. The speaker has a baffle diameter of 45 mm, an effective piston area of 12.5 cm^2, and a maximum power of 3 W. Its recommended frequency response range is between 250 Hz and 10 kHz. The speakers are controlled individually so they can be turned on and off separately.

Each speaker faces a different exit of the pipe at a distance of 0.6 m from each opening. Subsequently, the speakers are positioned parallel to the pipe axis, as shown in Fig. 3. The sound played by the speakers is white noise so that all frequencies are excited simultaneously. Moreover, both speakers play a different white noise audio file to avoid coherence.

Measurements are repeated for two pipes of different diameters; one with a diameter of 0.45 m (referred to henceforth as big pipe) and the other with a diameter of 0.2 m (referred to as small pipe). Both pipes have the same length of 1.5 m. Furthermore, measurements are performed with and without an acoustic-absorbing foam layer in the middle of the pipe. For both pipes, a circular foam layer of the same diameter as the pipe is created by sticking 6 layers of thinner insulation foam on top of each other, achieving a total thickness of 0.1 m. The acoustic-absorbing material used is melamine foam, which is a material commonly used for insulation [1]. The insulation foam circle is placed in the middle of the pipes to prevent leakage of the sound emitted by one speaker positioned on one side of the pipe to the other. This allows the sources to be isolated so that the breakdown of multiple sources can be compared to a single source.

A series of measurements is performed for each pipe with and without foam for comparison purposes. The tests performed for each configuration are listed in Table 1. In this example, the tests are performed for the big pipe and no foam between the speakers. The same measurements are repeated for the big pipe with foam and the small pipe with and without insulation foam.

[1] https://www.akoestiekwinkel.nl/flamex-basic-akoestische-platen

Table 1: Tests performed per configuration. In this case the pipe configuration is the big pipe, without foam. The values -4 and -10 indicate the decrease in dB of the right speaker volume

meas nr.	left	right	duration (s)
Big Pipe, No foam			
1 background	off	off	10
2	on	off	30
3	off	on	30
4	off	-4	30
5	off	-10	30
6	on	on	30
7	on	-4	30
8	on	-10	30
9 tap test	off	off	10

The acoustic data is recorded for 30 s at a sampling frequency of 50 kHz, using a linear microphone array consisting of 52 PUI Audio POM-2735P-R analog condenser microphones[2]. The microphones have a sensitivity of -35 $\pm$ 2 dB (ref. 1 V/Pa) and a frequency range of 20 Hz to 25 kHz. The microphones are connected to a data acquisition system (DAQ), which is connected to a laptop to record the data. The microphones have an equidistant spacing d of 0.12 m, providing a total length of 6.12 m. As a result, using Eq. (1), grating lobes are expected for wavelengths smaller than 0.24 m or frequencies higher than 1.4 kHz. The microphones are taped to thin wooden planks, which are positioned 2.75 m away and parallel to the pipe axis, see Fig. 1. Two additional microphones are placed at the exits of the pipe as reference microphones, as shown in Fig. 2.

$$d = \frac{1}{2}\lambda \tag{1}$$

[2]https://puiaudio.com/product/microphones/pom-2735p-r

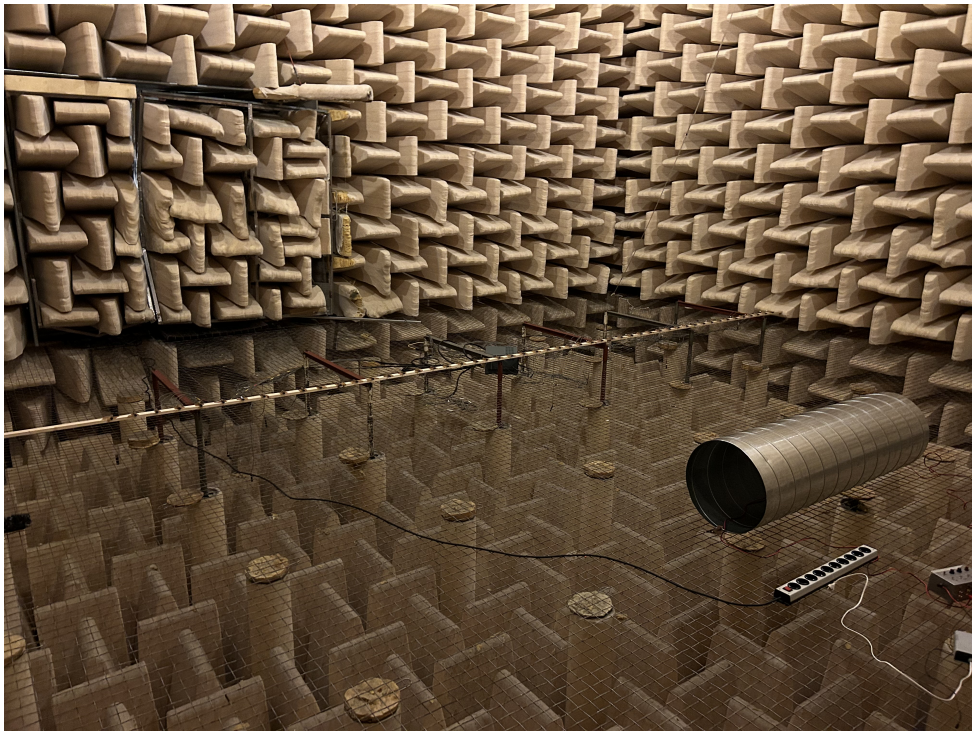

Figure 1: Experimental setup with the microphone layout inside of the anechoic chamber.

Figure 2: The reference microphone is placed at the exit of the pipe.

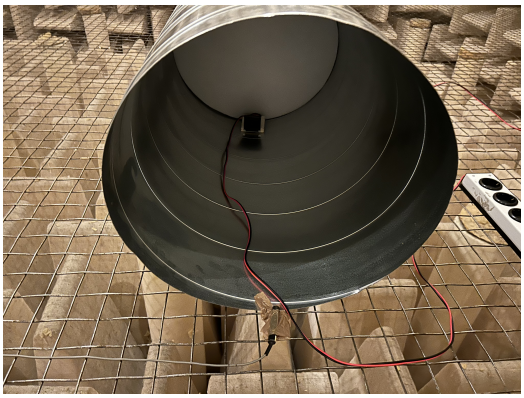

Figure 3: Speaker and insulation foam placement inside the big pipe. The foam is positioned in the middle of the pipe and the other speaker is positioned in the same manner on the other side of the foam layer.

3 METHODOLOGY

The data from the experiments is post-processed to obtain acoustic source maps. The source maps are calculated with the following methods: Conventional Frequency Domain Beamforming (CFDBF), DAMAS [4], and CLEAN-SC. Additionally, CLEAN-SC is also used for a directivity breakdown.

For all methods, the acoustic pressure data recorded by each microphone is converted from the time domain to the frequency domain, using a Fourier transform. Moreover, the data is split into snapshots of 5000 samples (0.1 s), where each snapshot overlaps by 50%. Subsequently, Hanning weighting is applied to minimize spectral leakage. Next, for each snapshot, the cross-spectral matrix (CSM, $\mathbf{C}$) is computed by multiplying the pressure amplitudes in the frequency domain by their complex conjugate transpose (indicated by *). The CSM is then obtained by averaging the CSM over all the snapshots:

$$\mathbf{C} = \langle \mathbf{p}_e \mathbf{p}_e^* \rangle \tag{2}$$

where e indicates the snapshot number and for each snapshot e and frequency f, $\mathbf{p}_e$ is given by:

$$\mathbf{p}_e(f) = \begin{pmatrix} p_1(f) \\ \vdots \\ p_{N_{mic}}(f) \end{pmatrix}, \tag{3}$$

where p_n is the pressure at each microphone for n = 1,..., N_{mic} microphones.

3.1 Conventional Frequency Domain Beamforming (CFDBF)

Conventional frequency domain Beamforming (CFDBF) is a frequency domain method and is the most straightforward way to process phased array data [11], as it is fast and robust. The source pressure is modelled at a grid point ξ using the steering vector $\mathbf{g}$ and the source amplitude A. The components g_n model the expected phase variation over the array for a given source position. There are different formulations for the steering vector in the literature depending on the application [1, 10]. For a stationary monopole point source [5] the steering vector can be written as:

$$g_{j,n} = \frac{e^{\left(-2\pi i f \Delta t_{j,n}\right)}}{4\pi \left\| \mathbf{x}_n - \xi_j \right\|} = \frac{exp\left[\frac{-2\pi i f \left\| \mathbf{x}_n - \xi_j \right\|}{c}\right]}{4\pi \left\| \mathbf{x}_n - \xi_j \right\|}, \tag{4}$$

where, c is the speed of sound, $i^2 = -1$, $\mathbf{x}_n = (x_n, y_n, z_n)$, n = 1,..., N_{mic}, $\Delta t_{j,n}$ is the time delay between reception at $\mathbf{x}_n$ and emission at ξ_j, so $||\mathbf{x}_n - \xi_j||$ represents the distance between the source and receiver. The aim is to obtain the source power A at grid point ξ_j by minimizing the difference between the recorded pressure and the modelled pressure:

$$minimize\left(||\mathbf{C} - A\mathbf{g}_j\mathbf{g}_j^*||^2\right) \tag{5}$$

Solving for the source power gives:

$$A(\xi) = \frac{\mathbf{g}_j^* \mathbf{C} \mathbf{g}_j}{||\mathbf{g}_j||^4} \tag{6}$$

This expression is known as "Conventional Beamforming". Now Eq. (6) can be shortened by the introduction of the weighted steering vector at scan point ξ_j:

$$\mathbf{w_j} = \frac{\mathbf{g}_j}{\mathbf{g}_j^* \mathbf{g}_j} = \frac{\mathbf{g}_j}{||\mathbf{g}_j||^2}, \tag{7}$$

in that case Eq. (6) becomes Eq. (8):

$$A_j = \mathbf{w}_j^* \mathbf{C} \mathbf{w}_j \tag{8}$$

3.2 DAMAS

The Deconvolution Approach for the Mapping of Acoustic Sources (DAMAS) is a tool developed by Brooks and Humphreys to improve upon the CFDBF results by accounting for the presence of multiple sources. The tool solves the following inverse problem so that the source strength distributions are extracted from the CFDBF acoustic source maps [4]:

$$\mathbf{y} = \mathbf{A}\mathbf{x}. \tag{9}$$

The number of grid points is given by J, thus $\mathbf{y} \in \mathbb{R}^{J\times 1}$ with $\mathbf{y}$ representing the source power output obtained from the conventional beamforming, $\mathbf{x} \in \mathbb{R}^{J\times 1}$ is the so-called equivalent source distribution at the same grid locations. Because of finite resolution and sidelobes $\mathbf{x} \neq \mathbf{y}$. $\mathbf{A} \in \mathbb{R}^{J\times J}$ is the propagation matrix. Each column of $\mathbf{A}$ contains the point spread function (PSF) of that corresponding grid point j. Equation 9 is generally solved using a Gauss-Seidel iterative method [6], with the constraint that the source powers $\mathbf{x}$ are positive. This typically requires thousands of iterations to obtain a source map, which can become an issue for large $\mathbf{A}$ as the computation time scales scales with J^3. However, in the current study, computational time should not pose a problem, because a one-dimensional scan grid is used, which significantly reduces the amount of grid points required to provide the desired accuracy.

3.3 CLEAN-SC

CLEAN-SC is a frequency-domain deconvolution method developed by Sijtsma [11]. The method makes use of the fact that the main lobes are spatially coherent with their sidelobes. These sidelobes are removed from the CFDBF source maps in an iterative manner, to obtain a clean map. The CLEAN-SC method works in the following way.

For one frequency or a frequency band, a peak source is searched in the *dirty map* obtained from CFDBF. This peak source is then removed from the CSM and replaced by a clean beam (beam without sidelobes) in the *clean* source map. Afterwards, the degraded CSM is used to compute an updated dirty map, in which the first peak source has been removed. A new peak source is searched in the updated dirty map and again removed from the degraded CSM and a clean beam is added to the *clean* source map. This process is repeated until a stop criterion is reached. This criterion can be a maximum number of iterations or when the *clean* CSM contains significantly more information than the degraded CSM.

The process at each iteration can be written in terms of the following steps. The maximum value in the dirty map at scan point $\vec{\xi}_j$ is searched, which is equal to CSM multiplied by a set of weighted steering vectors $\mathbf{w}_j$:

$$max(A_j) = A(\vec{\xi}_j) = \mathbf{w}_j^* \mathbf{C} \mathbf{w}_j. \tag{10}$$

In this case, there is no distance correction in the steering vector, thus Eq. 7 becomes:

$$\mathbf{w}_j = \frac{\mathbf{g}_j}{N_{mic}} \tag{11}$$

The contribution of a sound source to the CSM can be expressed in terms of the *source component* $\mathbf{h}_j$, noted as Eq. (12). $\mathbf{h}_j$ can be seen as an improved version of steering vector $\mathbf{g}_j$, as it better represents the unknown source vector $\mathbf{p}_j$.

$$\mathbf{h}_j = \frac{1}{(A_j)_{max}} \mathbf{C} \mathbf{w}_j = \frac{\sum_{k=1}^{K} \mathbf{p}_k (\mathbf{p}_k^* \mathbf{w}_j)}{(A_j)_{max}}, \tag{12}$$

where K is the number of sources and $\mathbf{p_k}$ is the source vector from the k^{th} source. Using this definition of the source component $\mathbf{h}_j$, $\mathbf{p}_j \mathbf{p}_j^*$ can be estimated by Eq. (13):

$$\mathbf{p}_j \mathbf{p}_j^* = (A_j)_{max} \mathbf{h}_j \mathbf{h}_j^*. \tag{13}$$

This estimate is then multiplied with the loop gain ϕ, $0 < \phi \leq 1$ as a safety factor [11] and subtracted from the CSM. For this paper a loop gain of 0.1 is selected. So that the new degraded CSM for the next l^{th} iteration can be written as:

$$C^{(l)} = C^{(l-1)} - \phi A_{(j),max} \mathbf{h}_j \mathbf{h}_j^*. \tag{14}$$

After L iterations, the original complete CSM can be written as the summations of the source components plus the degraded CSM, which is denoted as $\mathbf{D}$, Eq. (15). If a sufficient number of iterations is performed $||\mathbf{D}^{(L)}|| << ||\mathbf{C}^{(L)}||$. This indicates that the clean CSM contains significantly more information than the degraded CSM. In that case, the complete CSM can be approximated by the first term on the right-hand side of Eq. (15):

$$\mathbf{C}^{(L)} = \phi \sum_{j=1}^{L} (A_j)_{max} \mathbf{h}_j \mathbf{h}_j^* + \mathbf{D}^{(L)} \approx \phi \sum_{j=1}^{L} (A_j)_{max} \mathbf{h}_j \mathbf{h}_j^*. \tag{15}$$

3.4 Directivity breakdown

In addition to creating the source map of the array data, CLEAN-SC can also be used to perform source power integration and directivity analysis. For each iteration l a maximum source was localized at the associated scan point ξ_j, hence the location of the source in the map is known. Moreover, if the source is static (so it is not moving in time), it is possible to assign sound sources to specified areas or parts. As a result, the CSM can be written as the sum of different sources from predefined areas, which is especially applicable to static engine noise testing. In that case, Eq. (15) can, for example, be written as a breakdown of engine noise sources (e.g. intake, bypass, core, and jet) as done by Sijtsma [13]:

$$\mathbf{C} = \left(\sum_k A_k \mathbf{h}_k \mathbf{h}_k^*\right)_{\text{intake}} + \left(\sum_k A_k \mathbf{h}_k \mathbf{h}_k^*\right)_{\text{bypass}} + \left(\sum_k A_k \mathbf{h}_k \mathbf{h}_k^*\right)_{\text{core}} + \left(\sum_k A_k \mathbf{h}_k \mathbf{h}_k^*\right)_{\text{jet}} . \quad (16)$$

In the same way, the sources in the current experiment can be split into left, right, and other:

$$\mathbf{C} = \left(\sum_k A_k \mathbf{h}_k \mathbf{h}_k^*\right)_{\text{left}} + \left(\sum_k A_k \mathbf{h}_k \mathbf{h}_k^*\right)_{\text{right}} + \left(\sum_k A_k \mathbf{h}_k \mathbf{h}_k^*\right)_{\text{other}} \quad (17)$$

Not only can sources be localized, but it is also possible to extract information about their directivity, by considering the individual diagonal elements of the CSM. This way, CLEAN-SC is capable of providing directivity information of separate source areas.

In order to provide a noise breakdown, the source areas have to be defined. For the DGEN380 static engine tests, the areas are dependent on individual noise sources of the engine, as displayed in Fig. 4a. In this case, the sources are not symmetric and therefore neither are the selected areas. However, in the case of the current experimental setup, the sources are symmetric, hence, it makes sense to define the areas symmetrically as displayed in Fig. 4b. The source areas are set at ± 0.15 m in each of the pipe exits.

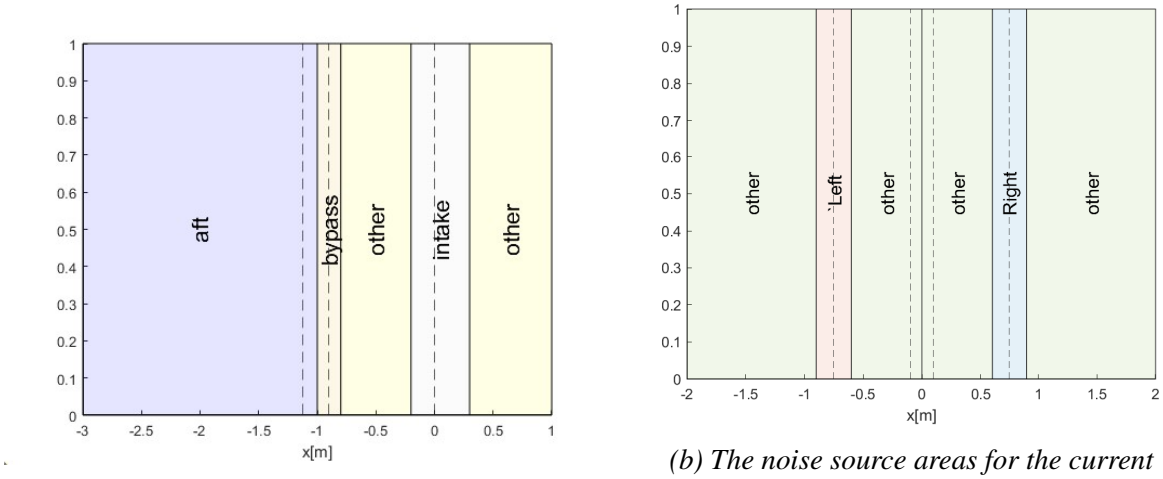

(a) The noise source areas adapted from [13]

(b) The noise source areas for the current experiment

Figure 4: The noise source areas, the dotted lines in (a) indicate from left to right; core exhaust, bypass exhaust, and intake [13], while in (b) they indicate; left pipe outlet, left speaker location, right speaker location, and right pipe outlet.

4 RESULTS AND DISCUSSION

The acoustic source maps are created for a frequency range from 500 Hz to 10000 Hz. This range is selected because below 500 Hz the speaker performance is unreliable. The spatial resolution also decreases at lower frequencies due to the Rayleigh resolution limit [2]. Acoustic

source maps are made up to 10 kHz, as this is the most relevant part of the spectrum, especially for engine noise. In addition, the case for the pipe with the larger diameter of 0.45 m is highlighted, as this case is more similar in size to an engine. Overall, similar findings apply to both pipes, unless explicitly stated in the text.

4.1 Source Maps

The source maps in Fig. 5 are computed using CFDBF. In both source maps, the left speaker is turned on and for Fig. 5a, there is no acoustic-absorbing foam placed inside the pipe, whereas for Fig. 5b there is insulation foam inside the pipe. The effect of the foam is visible when comparing both source maps. In Fig. 5a, there is leakage from the left side of the pipe to the right side, which is visible in the plot as the sources at the right exit of the pipe. In Fig. 5b, these sources are not present on the right side, indicating that there is negligible leakage when the insulation foam is inserted into the pipe.

Both acoustic source maps also contain a large number of grating lobes, especially for the side for which the speaker is turned on. Between 4000 Hz and 6000 Hz the grating lobes are similar in amplitude to the real source, which is undesirable, as it could lead to interpretation errors. The benefit of the current experiment is that the location of the sound sources is known, however, in engine testing in real-world conditions, this is not the case. Hence, a better method than CFDBF to distinguish actual sources from grating lobes is desired.

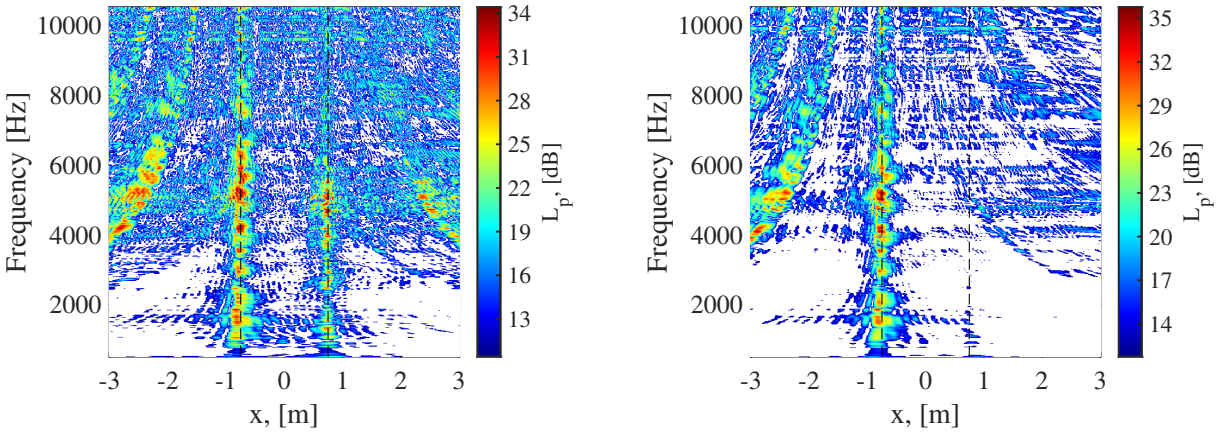

Figure 5: CFDBF acoustic source maps for the big pipe with (a) the left speaker on with no acoustic-absorbing foam and (b) with foam. The vertical black dotted lines indicate the exits of the pipe.

A method, which provides better-quality source maps is DAMAS. The source maps for the same cases as for CFDBF are shown in Fig. 6. These are obtained with 300 iterations and a grid resolution of 0.03 m. Again, the case of no foam and with foam with the left speaker on are compared. DAMAS does a better job at suppressing grating lobes compared to CFDBF. However, there are still grating lobes present in the plot, especially on the side on which the speaker is turned on. Furthermore, the effect of the foam can also be observed by comparing the sources at the right exit of the pipe in Fig. 6a and Fig. 6b. Once again, there is almost no

leakage visible in the source map, for the case with foam, indicating its effectiveness for sound absorption.

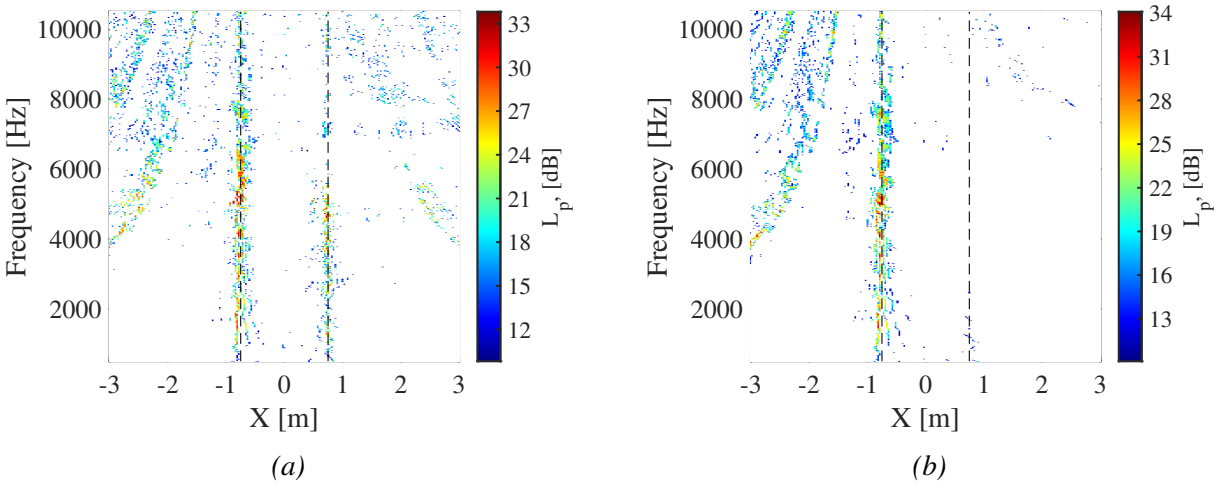

Figure 6: DAMAS acoustic source maps for the big pipe with (a) the left speaker on and no acoustic-absorbing foam and (b) with foam (b). The vertical black dotted lines indicate the exits of the pipe.

The main method used to analyze the experimental data in this study is CLEAN-SC. The source maps obtained using the CLEAN-SC method for cases with and without acoustic-absorbing foam are shown in Fig. 7 for the left speaker on and for the right speaker on in Fig. 8. Figure 9 shows the acoustic source maps for both speakers on, with and without foam. In general, the source maps are cleaner than the maps from DAMAS and much better than the maps from CFDBF. Nonetheless, in all acoustic source maps, there are still some grating lobes visible, especially for frequencies above 8000 Hz.

In the acoustic source maps corresponding to the left speaker on, see Fig. 7, it seems that the sources at the left exit are not perfectly in line with respect to the exit location indicated in the plot. This is most likely caused by a small mismatch between the assumed pipe location in the plot and the actual location in the experiment. This shift is not present in the source maps with the right speaker on, see Fig. 8.

Another noticeable aspect when comparing the left side to the right side is that the left speaker appears to be louder than the right speaker between 5-10 kHz, while the right speaker appears to be louder below 5 kHz. This can be seen by comparing the source strengths on the left side to the right side in Fig. 9b, where both speakers are turned on and there is foam insulation in between the speakers. This fact is confirmed by the spectra measured by the reference microphones.

The CLEAN-SC acoustic source maps for tests with no acoustic-absorbing foam and one speaker turned on, are shown in Fig. 7a for the left speaker on and in Fig. 8a for the right speaker on. In both maps leakage to the opposite side of the pipe is visible. Also for CLEAN-SC, the algorithm can only select a source at the left or the right exit, because it relies on spatial coherence of the sources. For example, in Fig. 7a, this effect is visible around 4000 Hz. The algorithm selects sources on the right exit and, as a result, there are no sources present at the left exit for that frequency, as CLEAN-SC considers those sources as spatially

coherent sidelobes.

Now, would this have any implications for static engine noise tests? When leakage occurs in a turbofan engine, it is most likely not perceived as fully coherent, due to the highly-varying sound propagation environment. So when leakage occurs, CLEAN-SC will most likely treat the leakage as a new source, at the location of the leakage. The most likely case in which leakage could be coherent is when fan tones radiate through the bypass. Sijtsma solves this issue by removing shaft order tones from the microphone signal [13]. However, the fact that CLEAN-SC treats leakage as a potential new source introduces another issue, namely, that the source can contribute to a different source region, depending on how the integration areas have been defined. For example, when broadband compressor noise leaks through the back of the engine, CLEAN-SC would register a new sound source. However, since it is at the back of the engine the source would most likely lie in the area of the core or the exhaust. So its contribution to the noise source breakdown will fall under these areas, even though it originated from the compressor. It is, nevertheless, unlikely that noise from the compressor will leak to the back of the engine or that it has a large contribution to the total noise of the core or the jet. Therefore, this is most likely not an issue for the overall analysis. However, it also highlights why it is difficult to separate the core and the jet noise, as they are very close to each other, in addition to the fact that configurations with diffraction edges make the edges function as a new sound source.

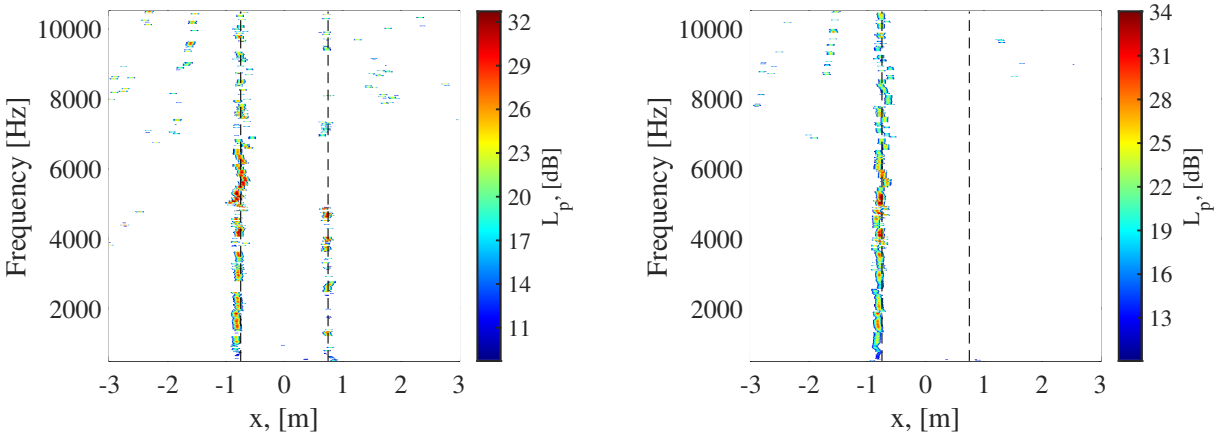

Figure 7: CLEAN-SC acoustic source maps for the big pipe and the left speaker on (a) without foam and (b) with foam (b). The black dotted lines indicate the exits of the pipe.

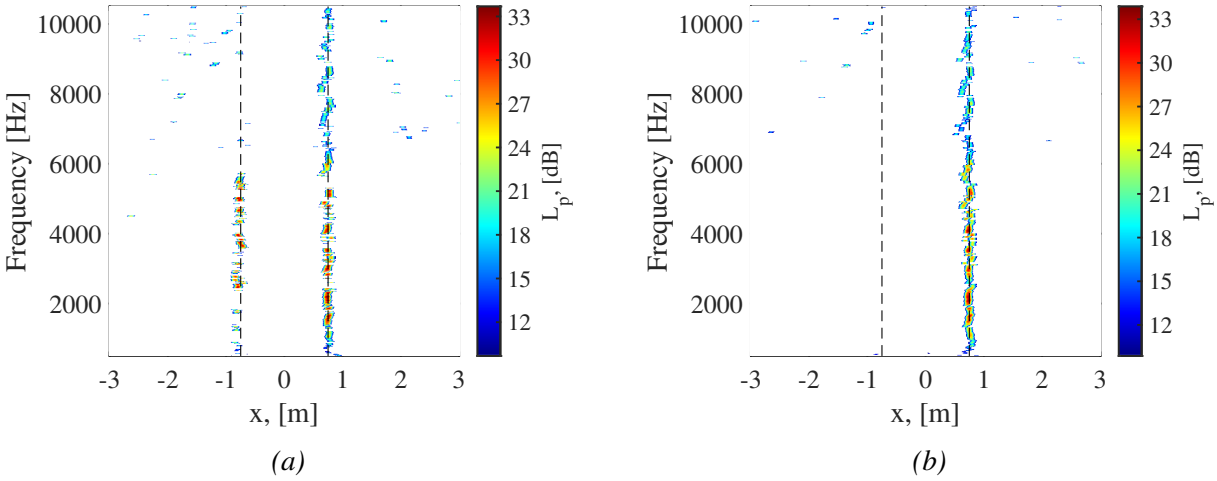

Figure 8: CLEAN-SC acoustic source maps for the big pipe and the right speaker on (a) without insulation foam and (b) with insulation foam. The black dotted lines indicate the exits of the pipe.

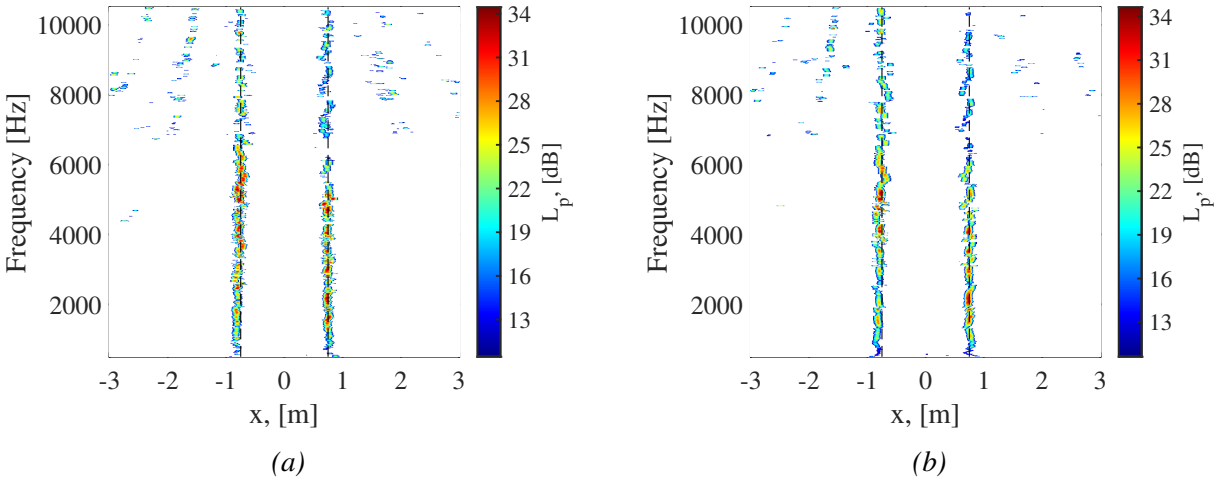

Figure 9: CLEAN-SC source map for the big pipe with both speakers on (a) without insulation foam and (b) with insulation foam (b).

4.2 Directivity breakdown

The acoustic source maps from CLEAN-SC are also used to perform the directivity breakdown. As explained in section 3, the CSM is decomposed into contributions from separate source areas. By considering the diagonal elements, information about the directivity is extracted and a noise source breakdown can be performed. The source areas employed are defined as depicted in Fig. 4b, where both the left and the right area cover ± 0.15 *m* from each of the exits of the pipe, providing a total width of 0.3 m. The rest of the sources fall into the category *other*. The directivity breakdown is performed for one-third-octave bands centered around a selected frequency. For instance, in Fig. 10, the directivity breakdowns for a one-third-octave band

centered at 3150 Hz are depicted for the left speaker on and the right speaker on. In these figures, the lines correspond to the respective contributions of the areas in Fig. 4b. Subsequently, the category *all* corresponds to the total sum of the noise levels from all areas. The overall analysis is limited to 5000 Hz due to the fact that at higher frequencies the microphones suffer slight amplitude off-sets.

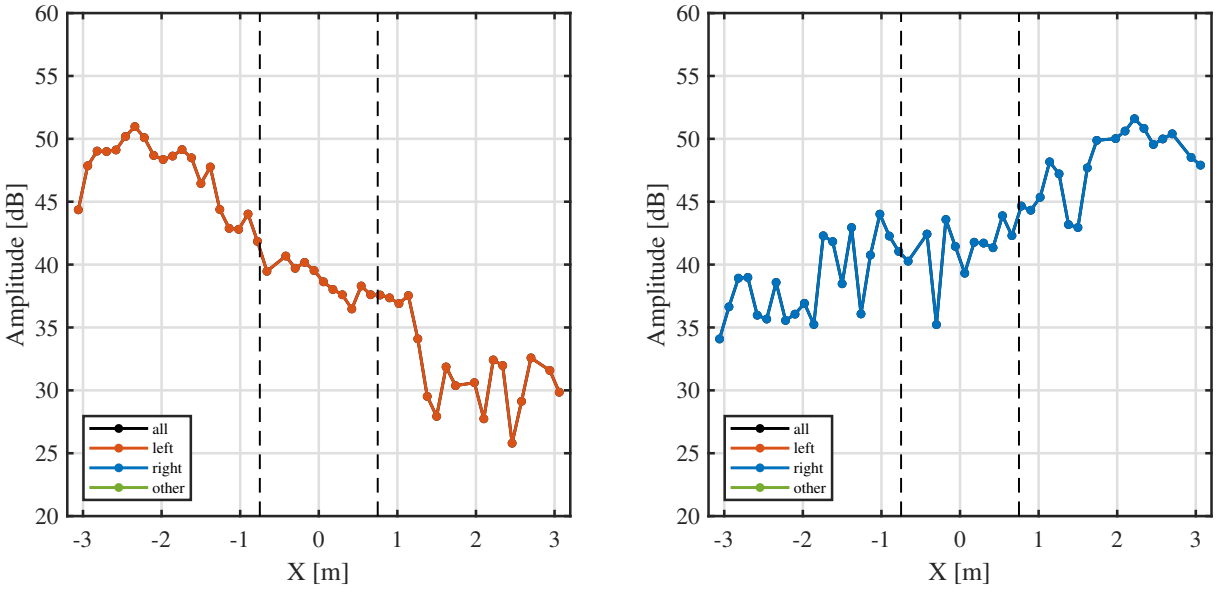

Figure 10: CLEAN-SC noise directivity breakdown for a one-third-octave frequency band centered at 3150 Hz for the big pipe with insulation foam and (a) the left speaker on and (b) the right speaker on.

When investigating the directivity breakdown for the left speaker at 3150 Hz in Fig. 10a, the results are as expected, i.e. the *left* and the *all* lines coincide, indicating that there are no other visible contributions from other areas. The source map in Fig. 7b confirms that there are no other sources at 3150 Hz apart from those located at the left exit. Hence, CLEAN-SC is able to isolate the sources and their contributions for the simple single-source case. Moreover, the directivity breakdown shows most noise radiated on the left side, while, on the right side, the noise levels decrease. This makes sense as only the left speaker is turned on and the foam stops leakage through the pipe. Subsequently, in Fig. 10b, only the right speaker is turned on and the breakdown follows a similar pattern. In this case, most noise is on the right side and the noise level decreases towards the left.

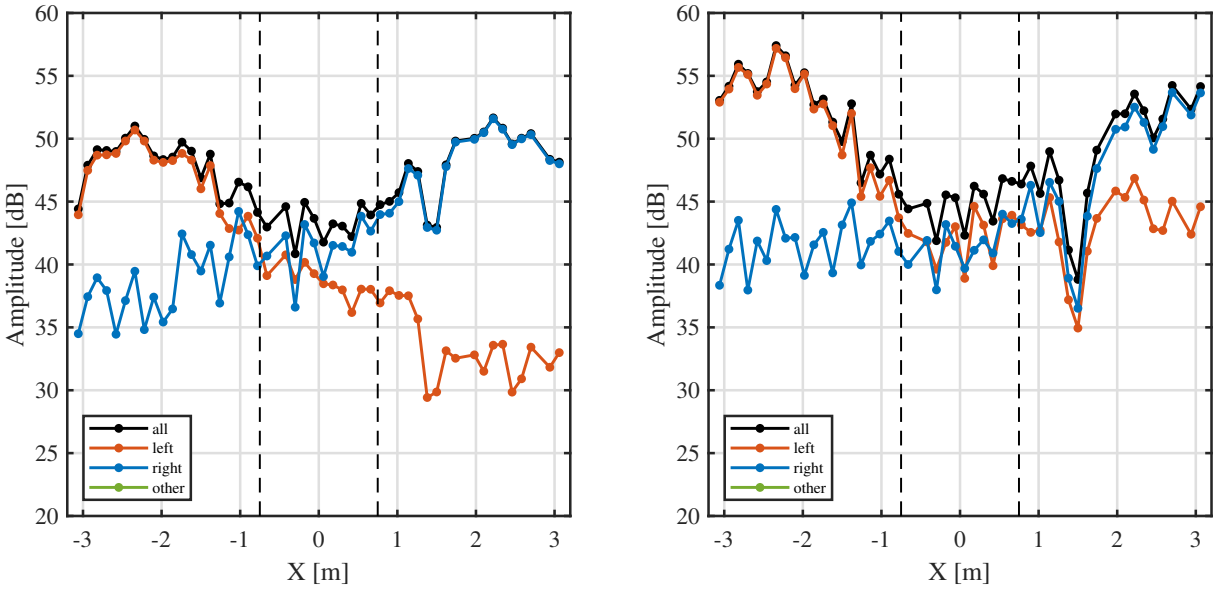

Figure 11: CLEAN-SC noise directivity breakdown for the big pipe with insulation foam and both speakers on for a one-third-octave frequency band centered at (a) 3150 Hz and (b) 5000 Hz.

The directivity breakdown can also be performed for the more challenging case with both speakers on. In Fig. 11 the breakdown for both speakers on is shown, where the breakdown in Fig. 11a corresponding to a one-third-octave-band centered at 3150 Hz and Fig. 11b is for 5000 Hz. The results for both frequency bands are as expected. CLEAN-SC is able to differentiate the sources and perform the directivity breakdown of these sources. On the left side, the left sources are dominant and on the right side, the right sources are dominant. Subsequently, as discussed earlier the right speaker outperforms the left speaker below 5000 Hz, which results in the sources on the right being a bit louder for 3150 Hz, while for 5000 Hz this is the other way around and the left speaker is louder.

Now, the main goal of this study is to assess whether CLEAN-SC is capable of performing an accurate directivity breakdown when multiple sources are present. Therefore, the breakdown of the case with just the left speaker on is compared (and used as a reference) to the breakdown of the left speaker with both speakers on. Essentially, Fig. 10a is compared to the contribution of left sources in Fig. 11a.

The comparison of the results is depicted in Fig. 12a. The case with one speaker on is represented by the blue line and functions as the baseline. The red line is the contribution of left noise sources when both speakers are on. Thus, by comparing the lines it can be determined if the directivity breakdown is still accurate when another source is present. It can be observed that on the left side, the lines are almost identical, which means that the breakdown is considerably accurate. However, on the right side, a larger deviation is observed between both results. This indicates that on the side where the other source is dominant, it is more difficult to separate the contribution of the left speaker from the noise of the right speaker, while for the section in the middle of the pipe, where neither the left nor the right speaker is dominant, the difference

between the lines fluctuates between both cases. Subsequently, the difference in sound pressure level between both cases is plotted in Fig. 12b, where this pattern is visible. In this instance, a positive amplitude difference indicates that the baseline is lower than the case to which it is compared, while a negative difference indicates that the baseline is higher than the other case.

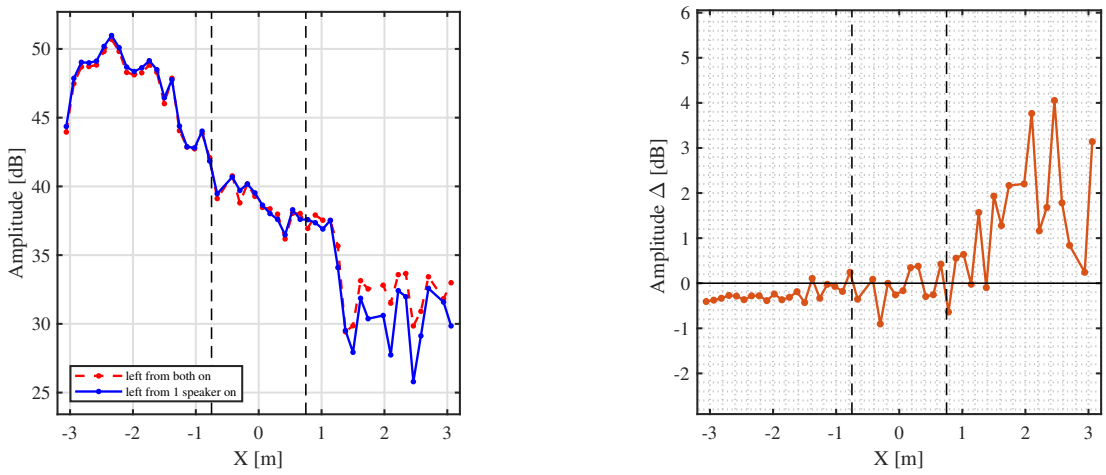

(a) *(b)*

Figure 12: (a) Directivity breakdown comparison for a one-third-octave frequency band centered at 3150 Hz of the left speaker on to both speakers on for the big pipe with foam and (b) the amplitude difference between the cases.

Similar to the analysis on the left side, sources from the right source can also be compared, which is depicted in Fig. 13. In this case, results are shown for a one-third-octave band centered at 3150 Hz, for the right speaker on compared to the right side of both speakers on. A similar pattern is visible, where CLEAN-SC is again able to accurately break down the sources on the dominant side (the right side in this case). In the middle section of the pipe, the variations start to fluctuate more. While on the side where the right speaker is not dominant, the results deviate more from the baseline.

Furthermore, the directivity breakdown is also analysed for more frequencies. The difference in amplitude of the breakdown of the left speaker on and the left side of both speakers is shown in Fig. 14a for 1000 Hz and in Fig. 14b for 5000 Hz. In these cases, the left side is the dominant side. Once again, it can be observed that for both cases the amplitude difference is small on the dominant side and that the amplitude difference increases on the non-dominant side. Additionally, the amplitude difference is larger at 5000 Hz, compared to the other two examples 1000 Hz or 3150 Hz.

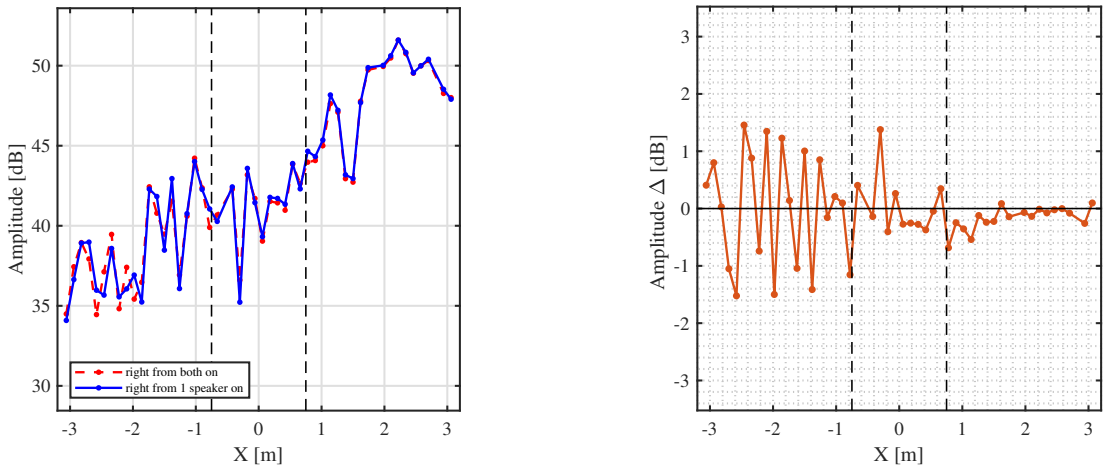

(a) (b)

Figure 13: (a) Directivity breakdown comparison for a one-third-octave frequency band centered at 3150 Hz of the right speaker on to both speakers on for the big pipe with foam and (b) the amplitude difference between the cases.

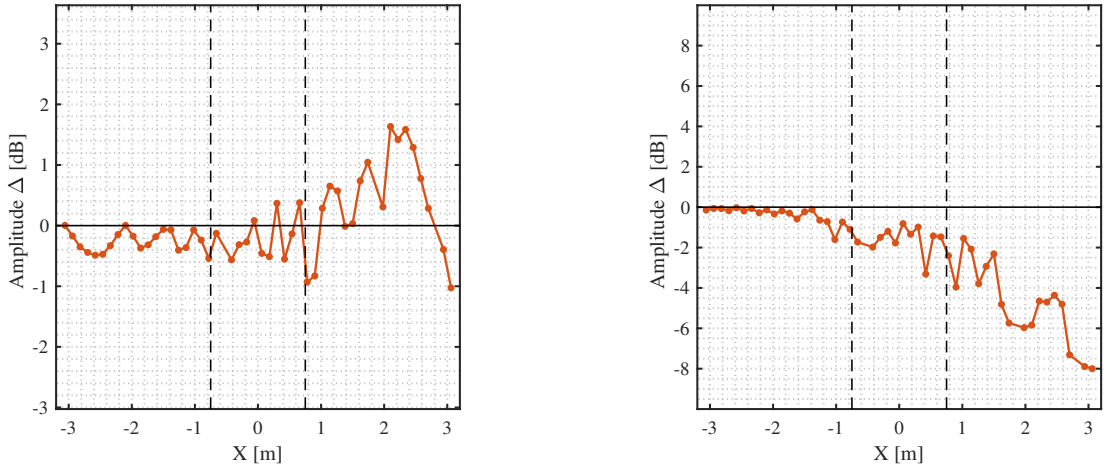

(a) (b)

Figure 14: Amplitude difference of left speaker on compared to both speakers on, for the big pipe with foam, for a one-third-octave frequency band centered at (a) 1000 Hz and (b) 5000 Hz.

4.3 Detailed analysis of directivity breakdowns

In order to obtain a better overview of the performance of CLEAN-SC for multiple frequencies, the Root Mean Square (RMS) of the amplitude difference is computed for three separate sections; left, middle, and right.

The sections are defined in Table 2, where the coordinates correspond to the locations of the microphones. By splitting the breakdown into sections the dominant side, the middle, and the

non-dominant side can be analysed separately. Otherwise, the RMS of the non-dominant side would dominate the total average, because the amplitude differences on the non-dominant side are significantly larger compared to the dominant side or the middle, despite being less relevant for the study.

The RMS indicates how much the amplitude differences between two cases deviate from zero (the ideal case). This RMS can be plotted for a range of frequencies and the overall breakdown capability of CLEAN-SC can be assessed per section over a frequency range. The RMS is computed using Eq. (18). $\Delta_N(f)$ is the difference between the red and the blue line for a certain frequency f and for a section, ranging from the locations in Table 2, where N indicates the microphone number. $N_{mic,sec}$ represents the number of microphones in a section.

Table 2: Sections considered for RMS-analysis. The X-coordinates and indices of the microphones, where the sections start and end.

Section	Start, X [m]	End, X [m]	$N_{mic,start}$	$N_{mic,end}$
Left	-3.06	-1.14	1	17
Middle	-1.02	1.02	18	34
Right	1.14	3.06	35	49

$$RMS(f) = \sqrt{\frac{1}{N_{mic,sec}} \sum_{N=N_{start}}^{N_{stop}} (\Delta_N(f))^2} \tag{18}$$

The RMS plots of the amplitude difference in directivity breakdown between one speaker on and both speakers on for the big pipe with foam are shown in Fig. 15a for the left side and in Fig. 15b for the right side. When comparing the left side to the right side, two aspects stand out. Firstly, in the frequency range from 0.5 kHz to 3 kHz the RMS of all sections of the left side is larger than the right side, especially around 1.5 kHz to 2 kHz, where there is a significant increase. Secondly, the RMS of the non-dominant section is larger for the left side case.

Furthermore, the same RMS plots but for the small pipe are depicted in Fig. 16a for the left side and in Fig. 16b for the right side. When comparing left to right for the small pipe, there appear to be larger peaks in RMS values for the left side in the frequency range between 0.5 kHz to 3 kHz compared to the right side, which are similar findings as those from the big pipe analysis. Subsequently, on the right side, the RMS increases significantly at 4.5 kHz for the dominant section and the middle section.

The exact cause of the deviations in RMS is difficult to pinpoint, as there is a variety of factors that could play a role. The CLEAN-SC algorithm is not perfect as demonstrated by the deviation increase for the non-dominant section. The algorithm has lower accuracy when the analysed source becomes a smaller part of the total noise. One of the reasons for this decrease in accuracy is that the noise level scales logarithmically with the measured pressure. Therefore, the contribution of the analysed source is several scales lower compared to the total measured noise. This can induces errors. In addition, the deviation can also be caused by speaker inconsistency, for example, it could be the case that the left speaker performs inconsistently between 1.5 kHz and 2 kHz, which leads to the larger deviation observed at that frequency. Another aspect that could play a role is the microphone performance.

In general, the average of the RMS of all dominant sections is below 1 dB as listed in Table 3. This indicates that CLEAN-SC is able to break down the noise with high accuracy even when another sound source is present. Subsequently, for the middle section, where no single source is dominant, the results are more variable depending on the frequency. In general, the deviation is larger compared to the dominant side, however, the average RMS value is still relatively low. Therefore, it can be concluded that CLEAN-SC is able to perform a directivity breakdown when no dominant source is present with a relatively low error of around 1 dB in this case. Moreover, as discussed before, it can be observed that the RMS of the breakdown increases for the non-dominant section. Therefore, for the non-dominant side, it can be concluded that the breakdown is not as reliable, as for the dominant side.

It should also be noted that these results are obtained for an area of ± 0.15 with respect to the pipe exits. The selected area has a large effect on the RMS. For example, if the area is decreased some sources that are not located exactly on the pipe exit could fall under a different source area and, therefore, these sources will in that case contribute to the category of *other* instead. For this experiment there are no other sources present next to the speakers, hence it is possible to define the areas with some margin. Hence, for static engine testing, the source areas should be defined carefully to obtain the best results.

Table 3: Average values of the RMS for the different sections in dB per plot

Section / RMS plot	Dominant	Middle	Non-Dominant
Big pipe left (Fig. 15a)	0.52	0.94	2.42
Big pipe right (Fig. 15b)	0.55	0.96	1.47
Small pipe left (Fig. 16a)	0.55	0.88	1.67
Small pipe right (Fig. 16b)	0.68	1.01	1.45

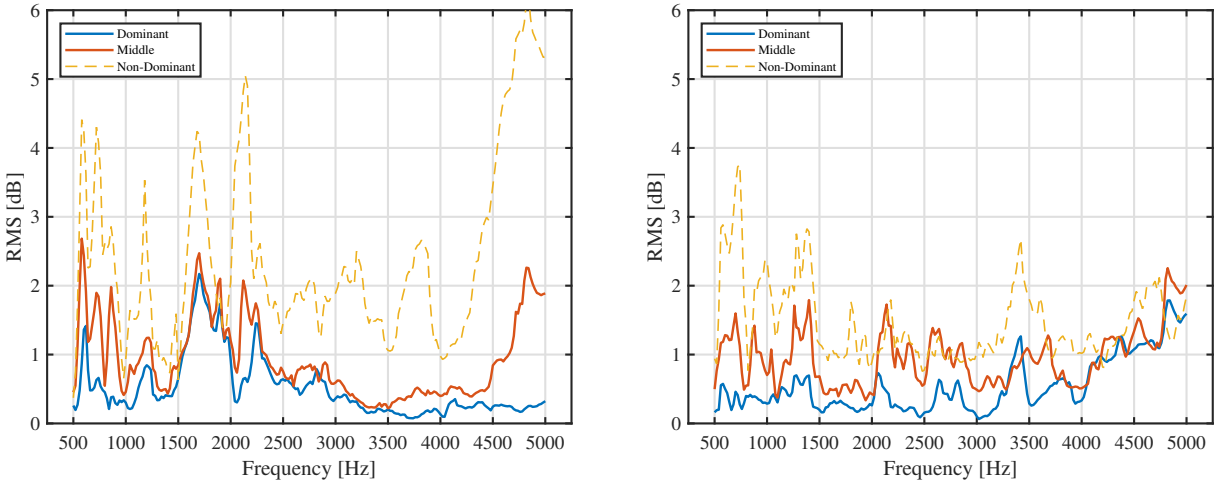

(a) *(b)*

Figure 15: RMS analysis results of the difference in directivity breakdown between one speaker on and both speakers on for the big pipe with foam for frequencies up to 5000 Hz for (a) the left speaker and (b) the right speaker.

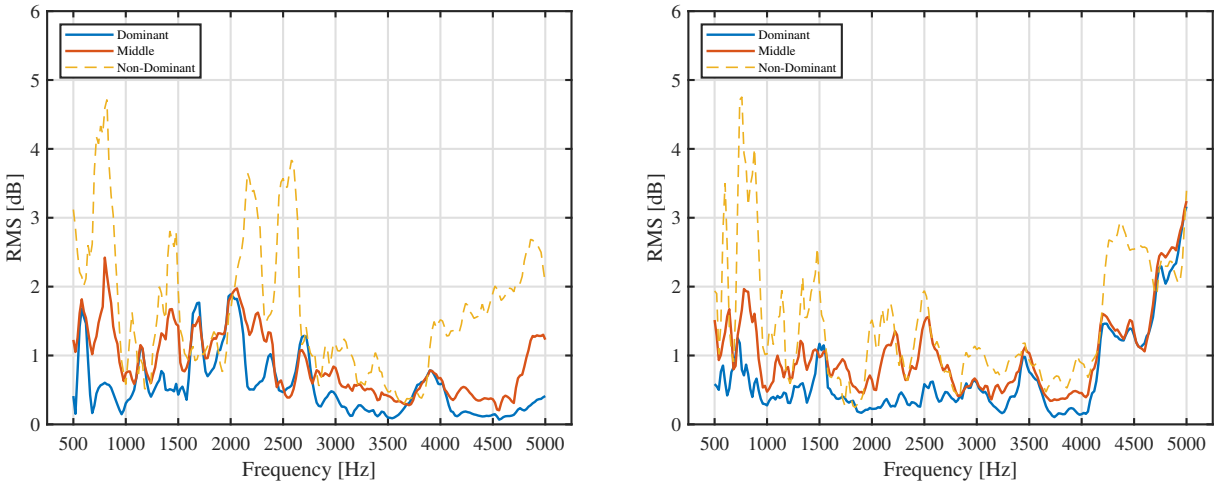

(a) (b)

Figure 16: RMS analysis results of the difference in directivity breakdown between one speaker on and both speakers on for the small pipe with foam for frequencies up to 5000 Hz for (a) the left speaker and (b) the right speaker.

5 CONCLUSIONS

In conclusion, the goal of this study is to investigate the directivity breakdown capabilities of CLEAN-SC and to determine whether this method is capable of obtaining reliable directivity breakdowns from microphone data of measurements in the far field.

In order to investigate this, experimental data is obtained by performing a number of tests in the anechoic chamber at the faculty of Applied Sciences at Delft University of Technology. In these tests, the location and directivity of the sources are measured separately, so that the results can be compared to the outcome of the deconvolution tool CLEAN-SC. The data from the experiments is analysed by making acoustic source maps using CFDBF, DAMAS, and CLEAN-SC. In addition, CLEAN-SC is also used to perform a directivity breakdown of the data.

The breakdown of a case with one source is compared to a case with multiple sources. The comparison of both breakdowns for a one-third-octave frequency band centered at 3150 Hz, it is shown that CLEAN-SC is able to perform a proper breakdown even when another source is present. Especially, for the dominant side the difference between both cases is small. Meanwhile, on the side where the source is not dominant, the deviation increases. To analyse a large number of frequencies the Root Mean Square (RMS) of the difference is computed. This analysis shows that CLEAN-SC is able to perform a breakdown of the dominant section with only a small deviation for the frequency range between 500 Hz and 5000 Hz. The deviation for the middle sections where no single source is dominant is larger, but still sufficiently low for useful analysis. For the non-dominant sections, the deviation is larger, which makes analysis unreliable.

Based on the results of this study, CLEAN-SC should be able to reliably perform directivity breakdown of microphone data of static engine tests, especially for the areas where the noise of the analysed part is either the dominant source or one of the dominant sources.

Recommendations

Future work could include tests with more than two speakers at multiple different locations. This way, the effect of the number of sources, their proximity, and their location on the directivity breakdown could be analysed. Furthermore, it would be interesting to apply other methods, such as AFINDS or SODIX that can also perform directivity breakdown to the experimental data, so that the performance of these more computationally-expensive methods can be compared to CLEAN-SC.

ACKNOWLEDGEMENTS

This publication is also a part of the *Listen to the future* project (project number 20247), a part of the Veni 2022 research programme (Domain Applied and Engineering Sciences) granted to Roberto Merino-Martinez and is also (partially) financed by NWO.

References

[1] T. Ahlefeldt, C. Spehr, T. Berkefeld, A. D. Marco, and L. Burghignoli. "A tomographic directivity approach to frequency domain beamforming." In *2018 AIAA/CEAS Aeroacoustics Conference*. 2018. doi:10.2514/6.2018-2808. URL https://arc.aiaa.org/doi/abs/10.2514/6.2018-2808.

[2] J. Allington-Smith. "Instrumentation — astronomical instrumentation." In *Encyclopedia of Modern Optics* (edited by R. D. Guenther), pages 281–296. Elsevier, Oxford, 2005. ISBN 978-0-12-369395-2. doi:https://doi.org/10.1016/B0-12-369395-0/00831-9. URL https://www.sciencedirect.com/science/article/pii/B0123693950008319.

[3] E.-L. Bertsch. *Noise Prediction within Conceptual Aircraft Design*. Ph.D. thesis, Deutsches Zentrum für Luft- und Raumfahrt Institut für Aerodynamik und Strömungstechnik, Braunschweig, 2013.

[4] T. F. Brooks and W. M. Humphreys. "A deconvolution approach for the mapping of acoustic sources (damas) determined from phased microphone arrays." *Journal of Sound and Vibration*, 294(4), 856–879, 2006. ISSN 0022-460X. doi:https://doi.org/10.1016/j.jsv.2005.12.046. URL https://www.sciencedirect.com/science/article/pii/S0022460X06000289.

[5] S. Glegg and W. Devenport. *Aeroacoustics of Low Mach Number Flows*. Elsevier Inc., 2017.

[6] R. M. Martinez. *Microphone arrays for imaging of aerospace noise sources*. Ph.D. thesis, Delft University of Technology, 2018. doi:https://doi.org/10.4233/uuid:a3231ea9-1380-44f4-9a93-dbbd9a26f1d6.

[7] R. Merino-Martinez, P. Sijtsma, A. Rubio Carpio, R. Zamponi, S. Luesutthiviboon, A. Malgoezar, M. Snellen, C. Schram, and D. Simons. "Integration methods for distributed sound sources." *International Journal of Aeroacoustics*, 18, 1475472X1985294, 2019. doi:10.1177/1475472X19852945.

[8] S. Oertwig, T. Schumacher, H. Siller, and S. Funke. "Extension of the source localization method sodix for coherent sound sources." In *AIAA AVIATION 2021 FORUM*. 2021. doi:10.2514/6.2021-2128.

[9] E. Peris. "Environmental noise in europe - 2020." Technical report, European Environment Agency, 2020.

[10] E. Sarradj. "Three-dimensional acoustic source mapping with different beamforming steering vector formulations." *Advances in Acoustics and Vibration*, 2012, 12, 2012. ISSN 292695. doi:https://doi.org/10.1155/2012/292695.

[11] P. Sijtsma. "Clean based on spatial source coherence." *International Journal of Aeroacoustics*, 6(4), 357–374, 2007. doi:10.1260/147547207783359459. URL https://doi.org/10.1260/147547207783359459.

[12] P. Sijtsma. *Acoustic beamforming for the ranking of aircraft noise*. Published in: Accurate and Efficient Aeroacoustic Prediction Approaches for Airframe Noise, VKI Lecture Series, 1 edition, 2013.

[13] P. Sijtsma. "Using clean-sc for determining the directivity of engine noise sources." In *AIAA AVIATION 2023 Forum*. AIAA AVIATION Forum, 2023. doi:10.2514/6.2023-3839. URL https://arc.aiaa.org/doi/abs/10.2514/6.2023-3839.

[14] B. J. Tester, S. Funke, K. M. Britchford, and C. J. Knighton. "Application of a noise source separation method (afinds) to external array measurements taken on short cowl engines in anechoic, outdoor, and indoor facilities." In *28th AIAA/CEAS Aeroacoustics 2022 Conference*, pages –. 2022. doi:10.2514/6.2022-2811. URL https://arc.aiaa.org/doi/abs/10.2514/6.2022-2811.

[15] Visaton – Speaker K 50 SQ – 8 Ohm. "http://www.visaton.de/en/products/fullrange-systems/k-50-sq-8-ohm." URL http://www.visaton.de/en/products/fullrange-systems/k-50-sq-8-ohm, accessed in March 2017.